ACS Photonics

Article

pubs.acs.org/journal/apchd5

Plasmon-Exciton Coupling in Symmetry-Broken Nanocavities

Rui-Qi Li,[†,‡] F. J. García-Vidal,[†,§] and A. I. Fernández-Domínguez*[,†]

[†]Departamento de Física Teórica de la Materia Condensada and Condensed Matter Physics Center (IFIMAC), Universidad Autónoma de Madrid, E-28049 Madrid, Spain

[‡]Key Laboratory of Modern Acoustics, MOE, Institute of Acoustics, School of Physics, Nanjing University, Nanjing 210093, People's Republic of China

[§]Donostia International Physics Center (DIPC), E-20018 Donostia/San Sebastián, Spain

Supporting Information

ABSTRACT: We investigate the onset of strong coupling in the temporal dynamics of the exciton population at a single emitter interacting with symmetry-broken plasmonic nanocavities. These structures consist in pairs of metallodielectric elements separated by a nanometric gap, with different degrees of asymmetry imposed on their geometric or material characteristics. In order to describe the emergence of plasmon-exciton-polaritons in these systems, we extend and generalize a transformation optics method previously applied to dimers of identical particles. This approach provides a natural decomposition of the spectral density in terms of a well-defined set of plasmonic resonances, as well as an insightful description of the coupling strength dependence on the emitter position. On the one hand, we shed light into the low sensitivity of plasmon-exciton interactions to geometric asymmetry in cavities such as nanoparticle-on-a-mirror configurations. On the other hand, our findings reveal that a more complex spatial and spectral dependence of the strong-coupling phenomenology takes place in systems with material asymmetry, such as two-metal and metal-dielectric dimers.

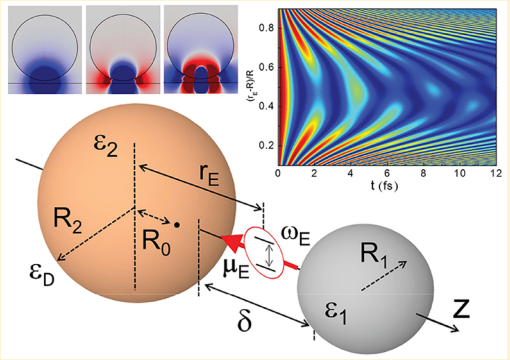

KEYWORDS: *surface plasmon, nanocavity, quantum emitter, exciton, strong coupling, transformation optics*

The interaction between quantum emitters (QEs), such as molecules or quantum dots, and surface plasmons (SPs) has attracted much attention lately as a key mechanism for the control of light through matter, and matter through light, at the nanoscale.[1,2] This interest originates from the ability of SPs to confine and amplify electromagnetic fields well below the diffraction limit of classical optics.[3] When the interaction between QEs and SPs enters the strong-coupling regime, both subsystems exchange energy within time scales shorter than their respective lifetimes. This leads to the emergence of plasmon−exciton−polaritons[4,5] (PEPs), hybrid states whose properties can be tuned through their light and matter content.

In the last number of years, much research efforts have focused on the theoretical[6−8] and experimental[9−13] investigation of PEPs at the macroscopic level (in systems involving large QE ensembles). This development has led to proposals for their exploitation in applications such as lasing,[14] catalysis,[15,16] and charge and energy transport.[17,18] Furthermore, plasmon−exciton interactions have been also thoroughly explored at the single emitter level,[19−21] although experimental evidence of PEPs in microscopic systems was not reported until very recently in nanoparticle-on-a-mirror[22] and bowtie[23] cavities. From a theoretical perspective, the coupling of SPs and single QEs has been addressed in simple geometries such as planar surfaces,[24] single nanospheres,[25,26] and distant particles.[27,28] Recently, we developed a transformation optics[29] (TO) approach for the description of PEPs in symmetric nanogap cavities.[30] This method allowed us to reveal that QE-SP coupling was strongly enhanced at highly asymmetric positions, far from the gap center.

In this Article, we extend our TO approach to further explore the role that asymmetry plays in the plasmon-exciton strong-coupling phenomenology. Specifically, we generalize it in order to investigate symmetry-broken nanocavities, in which asymmetry is imposed on geometry or material characteristics. Our method does not only account for the full richness of the plasmonic spectrum supported by the cavity, but also for the complex dependence of QE-SP interaction strength on the emitter position. This tool makes possible a quasi-analytical description of these systems, which naturally yields a self-consistent decomposition of the spectral density in terms of a complete set of SP resonances. The investigation of structures such as nanoparticle-on-a-mirror (NPoM) configurations allows us to gain insight into the low sensitivity of plasmon-exciton interactions to geometric asymmetry. On the other hand, we find that a more complex spatial and spectral dependence of QE-SP coupling takes place in cavities presenting material asymmetry, such as two-metal and metal-dielectric dimers.

Special Issue: Strong Coupling of Molecules to Cavities

Received: June 13, 2017
Published: October 19, 2017

DOI: 10.1021/acsphotonics.7b00616
ACS Photonics 2018, 5, 177−185

The text is organized as follows: First, we introduce our TO approach, which is subsequently applied to the calculation of spectral densities and exciton population dynamics. Next, we study PEP systems in which the asymmetry resides in the different sizes of the metal elements involved (including NPoM configurations). Finally, material asymmetry, specifically dimers composed of different metals and a metal and a dielectric medium, is investigated.

TRANSFORMATION OPTICS APPROACH

TO was initially conceived as a theoretical tool for controlling electromagnetic fields in the context of metamaterial science and technology.[29] Lately, this elegant framework was successfully applied to the description of SP-assisted phenomena such as light harvesting by nanoantennas,[31] Casimir forces between nanoparticles,[32] or the emergence of nonlocal effects in acute metallic geometries.[33] Importantly, the nanometric size of plasmonic systems allows their description within the quasi-static approximation. Here, we outline how TO ideas can be also used to treat the interaction between QEs and the SP spectrum supported by gap nanocavities. Figure 1 sketches the general

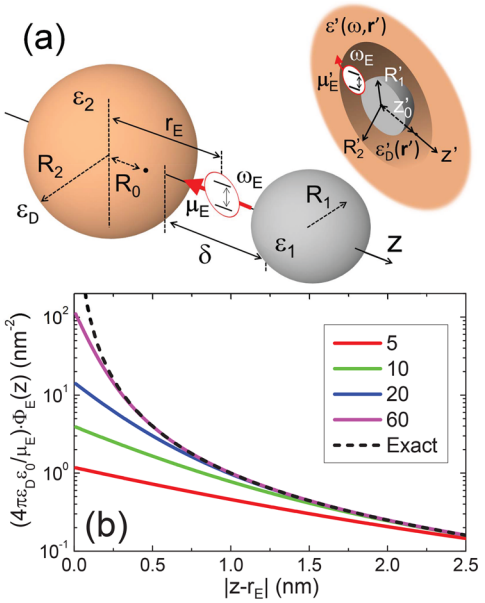

Figure 1. (a) Left: Sketch of the system under study: a single QE with transition dipole moment $\boldsymbol{\mu}_E = \mu_E\hat{\mathbf{z}}$ and frequency ω_E is placed at $z = r_E$ within the gap between two nanospheres. Right: Sketch of the geometry obtained from the inversion of the original system under eq 1. (b) QE source potential along the z-axis. The black dashed line plots the exact profile. Color lines correspond to the spherical harmonic expansion of the dipole potential up to different l_{max}.

system considered in this work: a single QE, modeled as a two level system with transition frequency ω_E, is placed at position $\mathbf{r}_E$ within the gap between two nanospheres of different frequency-dependent permittivities $\epsilon_1(\omega)$ and $\epsilon_2(\omega)$ and radii R_1 and R_2. The QE transition dipole moment $\boldsymbol{\mu}_E$ is parallel to the dimer axis (z-direction) and the whole system is embedded in a medium with dielectric constant ϵ_D.

Under an inversion of the form[34]

$$\mathbf{r}' - \mathbf{R}_0' = \frac{\Lambda^2}{|\mathbf{r} - \mathbf{R}_0|^2}(\mathbf{r} - \mathbf{R}_0) \tag{1}$$

where nonprimed (primed) coordinates correspond to the original (transformed) frame, the gap nanocavity can be mapped into the spherical concentric geometry depicted in the top right corner of Figure 1a. Whereas Λ is an arbitrary length-scale constant, the mapping requires the appropriate choice of the inversion point in the plasmonic cavity, $\mathbf{R}_0 = R_0\hat{\mathbf{z}}$ with $R_0 = \frac{l}{2} + \frac{R_2^2 - R_1^2 - \sqrt{\delta(\delta + 2R_1)(\delta + 2R_2)(2l - \delta)}}{2l}$ and $l = R_1 + R_2 + \delta$.

The spherical symmetry of the primed geometry allows solving Laplace's Equation in a quasi-analytical form, although the geometric convenience of the mapping also brings the complexity of spatially dependent transformed permittivities, $\epsilon'(\omega,\mathbf{r}') = \Lambda^2\epsilon(\omega,\mathbf{r}(\mathbf{r}'))/|\mathbf{r}' - \mathbf{R}_0'|^2$. It can be proven[35] that the quasi-static potential in the inverted system can be written as $\Phi'(\mathbf{r}') = |\mathbf{r}' - \mathbf{R}'_0|\phi'(\mathbf{r}')$, where $\phi'(\mathbf{r}')$ is a solution of Laplace's Equation in the primed frame. Thus, $\Phi'(\mathbf{r}')$ retains the azimuthal independence of the original quasi-static potential, and we can write

$$\Phi'(\mathbf{r}') = |\mathbf{r}' - \mathbf{R}_0'|\sum_{l=0}^{\infty}\left[a_l^+\left(\frac{r'}{R_0'}\right)^l + a_l^-\left(\frac{r'}{R_0'}\right)^{-(l+1)}\right]Y_{l0}(\theta', \varphi') \tag{2}$$

where $Y_{l0}(\cdot)$ denote spherical harmonics with $m = 0$. Equation 2 reduces the calculation of the scattered fields in the original frame to obtaining the expansion coefficients $a_l^{\pm}$ within the three spherical regions in the transformed structure. This is done by imposing the appropriate boundary conditions at the spherical interfaces. The continuity equations acquire a convenient tridiagonal form, where the coupling among coefficients with different l originates from the $|\mathbf{r}' - \mathbf{R}'_0|$ factor in $\Phi'(\mathbf{r}')$ (see ref 34). Once the coefficients are known, the quasi-static potential in the original frame can be calculated as $\Phi(\mathbf{r}) = \Phi'(\mathbf{r}'(\mathbf{r}))$. In the Supporting Information (SI), specific details on the TO approach for nanocavities presenting material asymmetry are provided.

The continuity equations discussed above need to be fed with the coefficients corresponding to the source of excitation. For a dipole source describing the QE located within the gap cavity, $\Phi_E(\mathbf{r}) = -\frac{1}{4\pi\epsilon_0\epsilon_D}\frac{\boldsymbol{\mu}_E(\mathbf{r} - \mathbf{r}_E)}{|\mathbf{r} - \mathbf{r}_E|^3}$ and the coefficients read

$$a_l^{E+} = \frac{\mu_E}{4\pi\epsilon_0\epsilon_D}\sqrt{\frac{4\pi}{2l+1}}\frac{\eta^2}{\Lambda^2\Delta}\left[1 + \frac{(l+1)\eta}{1-\eta}\right](1-\eta)^{-(l+1)},$$

$$a_l^{E-} = -\frac{\mu_E}{4\pi\epsilon_0\epsilon_D}\sqrt{\frac{4\pi}{2l+1}}\frac{\eta^2}{\Lambda^2\Delta}\left[1 - \frac{l\eta}{1-\eta}\right](1-\eta)^{l} \tag{3}$$

where $\eta = \Delta/(r_E - R_0)$, $\Delta = 2(l + R_1 - R_0)(2R_1 + R_2 - R_0)/[2l - R_0 - \delta]$. Figure 1b demonstrates the fast convergence of the expansion for the QE potential in absence of the nanocavity. We find that $\Phi_E(\mathbf{r})$ is converged at 1.5 nm distance with $l \leq l_{max} = 10$, whereas $l_{max} = 60$ is required to describe the potential at 0.2 nm. Throughout this article, we take $\epsilon_D = 2.13$, which corresponds to silica, used as a host dielectric in various plasmonic applications.[36] In order to analyze in detail and gain insights into the dependence of the strong coupling phenomenology on the complex plasmonic spectrum supported by the nanocavities, we consider a simple, idealistic model for the QEs: First, we take a rather large transition dipole moment, $\mu_E = 1.5\ e{\cdot}$nm, a value in agreement with recent experimental reports on 10−100 nm sized semiconductor quantum dots.[37] Second, we assume that the transition frequency, ω_E, can be swept across the optical regime. Finally, we neglect nonradiative decay in the excitonic dynamics (the QE quantum yield is set to 1).

DOI: 10.1021/acsphotonics.7b00616
ACS Photonics 2018, 5, 177−185

SPECTRAL DENSITY AND POPULATION DYNAMICS

The calculation of the expansion coefficients in eq 2 gives us access to the scattered electric field, $\mathbf{E}^{sc}(\mathbf{r}) = -\nabla\Phi_{sc}(\mathbf{r})$, in any position of the original frame. Through the evaluation of the z-component of the scattered electric field at $\mathbf{r} = \mathbf{r}_E$, we can calculate the Purcell enhancement experienced by the z-oriented QE at the gap of the nanocavity,[38]

$$P(\omega) = 1 + \frac{6\pi c}{\omega}\mathrm{Im}\{G^{sc}_{zz}(\omega, \mathbf{r}_E, \mathbf{r}_E)\} \tag{4}$$

where $G^{sc}_{zz}(\omega, \mathbf{r}_E, \mathbf{r}_E) = \frac{\epsilon_0}{\mu_E}\left(\frac{c}{\omega}\right)^2 E^{sc}_z(\omega, \mathbf{r}_E)$ is the zz entry of the scattered Dyadic Green's function at the QE position (note that for clarity, we have made explicit the dependence on frequency of the electric field). As we show below, the spectral density, $J(\omega)$, is the physical magnitude that controls QE-SP coupling and, therefore, the dynamics of the excitonic population at the emitter. This can be expressed in terms of the Purcell factor as

$$J(\omega) = \frac{1}{2\pi}\frac{\mu_E^2\omega^3}{3\pi\epsilon_0\hbar c^3}P(\omega) \tag{5}$$

Contrary to $P(\omega)$, $J(\omega)$ depends on the QE characteristics. It scales as μ_E^2, which makes QEs with large transition dipole moments convenient for strong coupling applications. Moreover, ω^3 factor in eq 5 increases the weight of the high frequency SPs with respect to $P(\omega)$.

Once the spectral density is known, the Wigner-Weisskopf problem[39] for the QE at the gap of the nanocavity can be solved. It establishes that the dynamics of the exciton population, $n(t) = |c(t)|^2$, at an initially excited QE $[n(0) = 1]$ is given by the integro-differential equation

$$\frac{dc(t)}{dt} = -\int_0^\infty d\tau \int_0^\infty d\omega J(\omega) e^{i(\omega_E-\omega)(t-\tau)}c(\tau) \tag{6}$$

Equation 6 accounts for the emergence of reversible dynamics in the excitonic population, characterized by the presence of oscillations in $n(t)$. This is the fingerprint of the onset of plasmon-exciton strong coupling and the emergence of PEPs in the system, which requires highly structured $J(\omega)$. Note that if the cavity presents a flat (unstructured) spectral density, $J(\omega) \simeq J(\omega_E)$, eq 6 yields $n(t) = e^{-2\pi J(\omega_E)t}$, which recovers the Purcell-enhanced monotonic decay characteristic of the weak coupling regime.

TO does not only provide an efficient method for the solution of eq 6. In ref 30, we showed that in the limit of vanishing gap, the continuity equations in the transformed frame can be written in diagonal form. This way, and using the high quality resonator approximation,[40] $J(\omega)$ for a pair of Drude metal spheres separated by a small gap can be expressed as a sum of Lorentz-like terms, each corresponding to a SP resonance sustained by the structure. Thus, this approach also allows for a convenient and efficient electromagnetic field quantization in lossy, open nanostructures.[41−43] Here, we extend this procedure to symmetry-broken cavities, and obtain quasi-analytical expressions for the frequencies, damping rates and the QE coupling strengths for the SPs supported by nanocavities with geometric and/or material asymmetry.

In order to illustrate the accuracy and to set the range of validity of our TO predictions, we use our approach to assess the performance of the same plasmonic dimer as a nanocavity, see Figure 2a, and as a nanoantenna, see Figure 2b. The structure

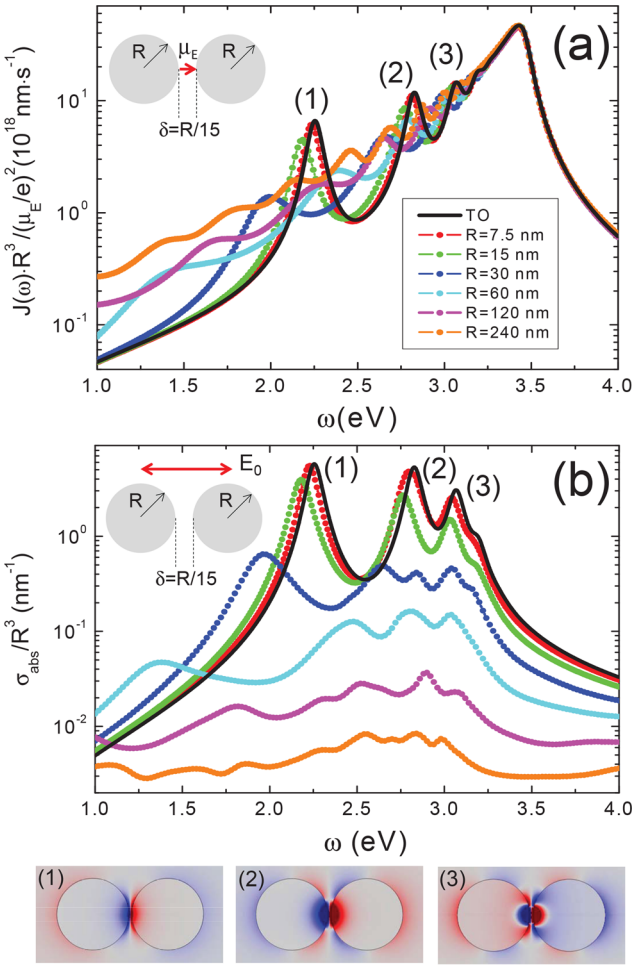

Figure 2. Spectral density (a) and absorption cross section (b) for pairs of identical silver spheres of various radii R separated by a gap $\delta = R/15$ (see insets). The cross-section (spectral density) is normalized to the (inverse of the) particles volume, R^3. Black lines plot TO quasi-static predictions (identical for all sizes), and color lines show full electromagnetics simulations. Insets: Color saturated surface charge maps (obtained via numerical simulations) for the three modes indicated in (a).

consists in two identical spheres of radius R separated by a gap $R/15$. Their Drude permittivity is given by $\epsilon(\omega) = \epsilon_\infty - \frac{\omega_p^2}{\omega(\omega+i\gamma)}$, with $\epsilon_\infty = 4.6$, $\omega_p = 9$ eV, and $\gamma = 0.1$ eV (fitted values for silver[8]). In both panels, quasi-static TO results (black solid line) are compared against full electromagnetics COMSOL Multiphysics simulations (color dots) for particle radii ranging from 7.5 to 240 nm. Figure 2a plots the spectral density, $J(\omega)$ for an emitter at the gap center, and Figure 2b shows the absorption cross section, σ_{abs}, under z-polarized illumination. Note that, in order to carry out a meaningful comparison between different R's, and taking into account the different scaling of both magnitudes, $J(\omega)$ is normalized to the inverse of the cavity volume (R^{-3}), and σ_{abs} to the cavity volume itself (R^3). We find that TO predictions for both quantities are in excellent agreement with simulations for small radius. As R increases, radiative effects become relevant, but they manifest in a very different way in both panels, being their impact on σ_{abs} much larger than in $J(\omega)$.

The contrast in the sensitivity to radiative losses of $J(\omega)$ and σ_{abs} is a consequence of the different plasmonic modes that play

DOI: 10.1021/acsphotonics.7b00616
ACS Photonics 2018, 5, 177−185

a relevant role in each magnitude. The three bottom panels in Figure 2 display color-saturated induced-charge density maps for the three lowest-frequency SP modes. These are the brightest (most radiative) ones, and their associated E_z^{sc}-fields are even with respect to the gap center. The spectral position of these modes is indicated in Figure 2a,b, which clarifies their contribution in each case. They show that σ_{abs} is governed by these low frequency SP resonances, greatly affected by radiation damping with increasing R. On the contrary, $J(\omega)$ presents a prominent maximum at frequencies well above these modes. This peak is extremely robust to radiation effects, which in turn are apparent around the lowest SP frequencies (the corresponding peaks red-shift, broaden and collapse as R increases). This high-frequency maximum in $J(\omega)$ can be considered as a pseudomode (PS) that, as we show below, originates from the spectral overlapping of a number of high-order, dark, SP resonances. In the following, we will see that $J(\omega_{PS})$ sets the intensity of plasmon-exciton interactions taking place in the nanocavity.

NANOCAVITIES WITH GEOMETRIC ASYMMETRY

In this section, we investigate symmetry-broken nanocativies at the geometric level. Specifically, we consider structures composed by elements of the same metal but different sizes, with special attention to the limiting case of NPoM. Figure 3a plots $J(\omega)$ evaluated at the center of the 2 nm gap between two spheres of different radii, R_1 and R_2 = 120 nm. As shown in Figure 2a, this particle size is beyond the validity of the quasi-static approximation at low frequencies. However, we anticipate that the accuracy of TO predictions around the pseudomode enables us to employ this framework to describe QE-SP coupling in ∼100 nm radius nanospheres. Taking the symmetric case ($R_1 = R_2$) as the reference, we find that $J(\omega)$ is considerably robust against variations in R_1/R_2. On the one hand, by decreasing R_1 the spectral maxima for the lowest-frequency SP resonances blue-shift. However, the PS maximum at high frequencies remains insensitive to this geometric asymmetry (a direct consequence of the localized nature of the SP modes forming it). It only decreases slightly for $R_1/R_2 = 0.01$. In this configuration, $R_1 < \delta$ and the spectral distance of the dipolar SP peak [labeled as (1) in Figure 2] and the PS is comparable to the Drude damping, γ = 0.1 eV. In fact, $J(\omega)$ in the vicinity of ω_{PS} resembles the spectral density for a single sphere ($R_1/R_2 = 0$). On the other hand, increasing R_1 red-shifts low-frequency SP resonances only very little, reaching the sphere-plane (or NPoM, $R_1 \to \infty$) limit already for $R_1/R_2 = 10$. Note that the radii of both spheres are at least 2 orders of magnitude larger than δ in this case.

The inset of Figure 3a displays $J(\omega)$ versus frequency and gap size for the NPoM geometry in the main panel. We focus on this cavity configuration because of its relevance in recent advances on the experimental probing of plasmon-exciton strong coupling.[22] The contour plot shows that $J(\omega)$ increases with decreasing δ, while the contributions from different SP modes red-shift and become discernible. For large gaps ($\delta/R_2 \sim 0.1$), all maxima merge at the PS position. Figure 3b,c renders the exciton population as a function of time and δ for a QE at resonance with the lowest SP mode (left) and with the PS (right). The population dynamics obtained from eq 6 reveals that the onset of QE-SP strong coupling takes place at $\delta \sim 3$ nm in both cases, and Rabi oscillations become apparent below this gap. Note that these gap sizes are comparable or smaller than the typical sizes of QEs with ∼1 e·nm transition dipole moments.[37] In a similar way as symmetric cavity configurations,[30]

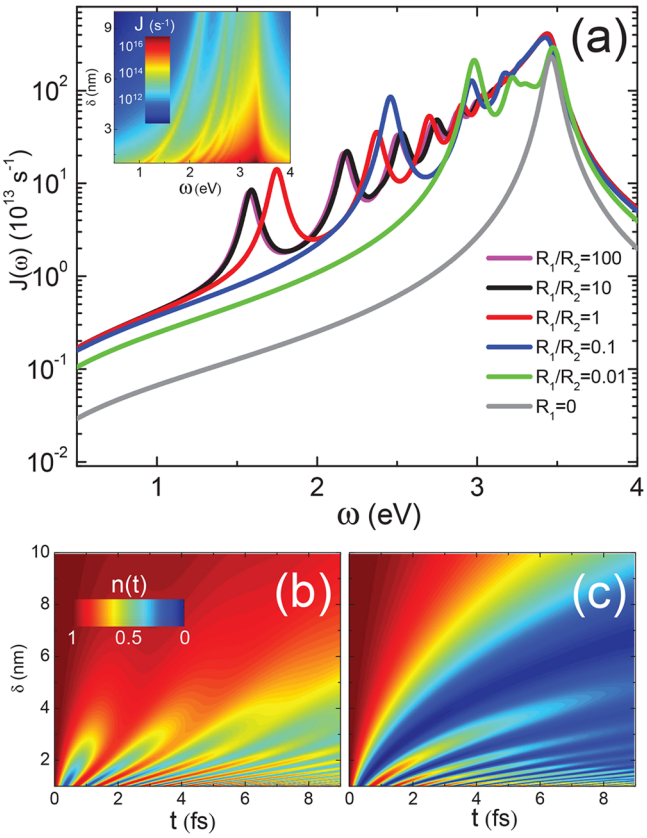

Figure 3. $J(\omega)$ at the center of the 2 nm gap between Ag nanoparticles of various relative sizes R_1/R_2 (R_2 = 120 nm). Inset: Spectral density versus frequency and gap size for $R_1/R_2 \gg 1$ (NPoM geometry). (b, c) Emitter excited state population versus time and gap size for the NPoM. The QE ($r_E = R_2 + \delta/2$) is at resonance with the lowest-frequency SP mode in panel (b) and with the PS in panel (c).

the resemblance between both panels allows us to infer that the mechanism controlling $n(t)$ is the same irrespective of ω_E. The analytical decomposition of $J(\omega)$ that follows indicates that this mechanism is the coupling to the PS maximum (see Figure 5), and that the small variations in the monotonic decay and the Rabi oscillation contrast originate from the different detunings ($\omega_E - \omega_{PS}$). Note that, as expected from the main panel of Figure 3a, the dependence of $n(t)$ with gap size for NPoM and symmetric cavities is rather similar.[30]

Next, we explore in detail the spectral density at the PS peak. Figure 4a plots $J(\omega_{PS})$ versus QE position along the cavity gap $(r_E - R)/\delta$ (for simplicity, we make $R_2 = R$ = 120 nm). Main panel (inset) corresponds to a NPoM (symmetric dimer) cavity with δ = 2 nm. Two different normalizations are considered. The black dashed line renders the ratio between $J(\omega_{PS})$ at $z = r_E$ and its value at the gap center. The spectral density increases in the same way as the QE approaches the nanosphere ($r_E = R$) and the flat metal surface ($r_E = R + \delta$), giving rise to a $\sim 10^2$ enhancement factor. To prove that this amplification is not due to proximity effects (the QE couples more strongly to the nearest metallic element), the red solid line plots $J(\omega_{PS})$ now normalized to the sum of the spectral densities for sphere and plane isolated. Three-orders of magnitude enhancements are found this way, which reveals that plasmonic hybridization amplifies greatly $J(\omega_{PS})$. The asymmetry in the spectral density profile in this case indicates that the contribution of SP hybridization to QE-SP coupling is slightly larger at the flat metal

DOI: 10.1021/acsphotonics.7b00616
ACS Photonics 2018, 5, 177−185

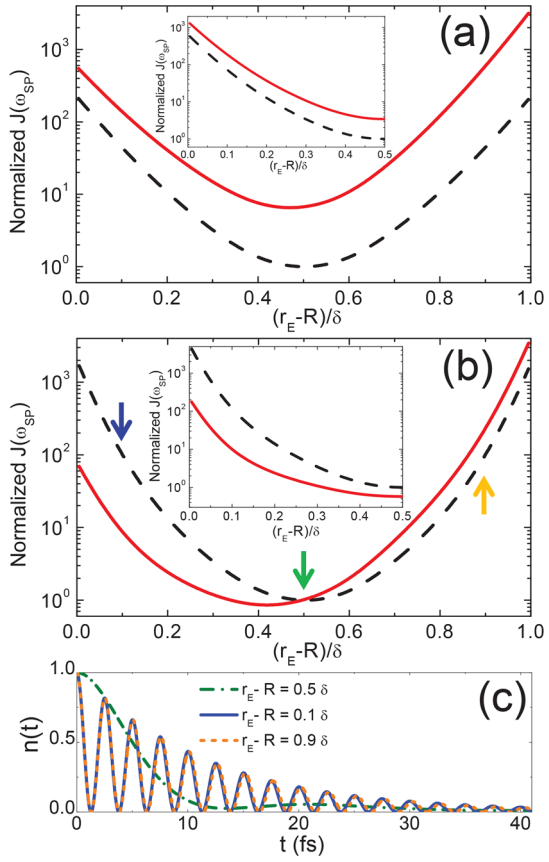

Figure 4. Spectral density at the pseudomode for sphere-plane (main panel) and symmetric sphere−sphere (insets) configurations (in both cases, $R_2 = R = 120$ nm) with $\delta = 2$ nm (a) and $\delta = 8$ nm (b). Black dashed lines plot $J(\omega_{PS})$ normalized to its value at the gap center. Red solid lines, $J(\omega_{PS})$ normalized to the sum of the sphere and plane isolated (both spheres in the insets). (c) $n(t)$ at $\omega_E = \omega_{PS}$ for the three different r_E's indicated by vertical arrows in panel (b).

surface, which compensates for the fact that the planar surface performs worse than a single metal sphere as a cavity by itself. The comparison between the main panel and the inset evidence again a clear similarity between the spatial dependence of $J(\omega_{PS})$ in NPoM and dimer geometries.

Figure 4b presents the same analysis as panel (a) but for a bigger gap size, $\delta = 8$ nm. This is a more realistic configuration for the realization of plasmon-assisted strong coupling phenomena, as QEs with large dipole moment could be placed in the nanocavity. We can observe that, in comparison with the 2 nm case, higher spectral density enhancements (relative to the gap center) can be achieved by displacing the QE position. Similarly, the asymmetry in the contribution of SP hybridization to $J(\omega_{PS})$ is also larger. Therefore, we can conclude that the impact that the emitter position has on QE-SP interactions increases with δ. In order to illustrate this effect, Figure 4c plots $n(t)$ for $\omega_E = \omega_{PS}$ at three different positions for the structure in panel (b). While the QE is only weakly coupled to the SPs at the gap center, it enters in the strong-coupling regime when displaced a distance $0.4\delta = 3.2$ nm. Despite the asymmetric geometry of the cavity, the exciton dynamics is exactly the same if the QE approaches the flat surface or the spherical particle.

As discussed above, our TO approach enables us to express the spectral density as a sum of Lorentzian contributions. For the case of a NPoM cavity, this decomposition reads

$$J(\omega) = \sum_{l=0}^{\infty} \sum_{\sigma=-1}^{1} \frac{g_{l,\sigma}^2}{\pi} \frac{\gamma/2}{(\omega - \omega_{l,\sigma})^2 + (\gamma/2)^2} \tag{7}$$

where the index l is inherited from eq 2 and refers to the multipolar order of the SPs. Furthermore, the index σ arises from the manipulation of the scattering coefficients. In the case of single metal nanocavities, it emerges naturally and can be associated with the even $(+1)$ or odd (-1) character of the SPs. The spectral width of all the terms in eq 7 is given by the Drude damping γ. The SP frequencies have the form

$$\omega_{l,\sigma} = \frac{\omega_p}{\sqrt{\epsilon_\infty + \epsilon_D \frac{\xi_l + \sigma}{\xi_l - \sigma}}} \tag{8}$$

with $\xi_l = [2 + \delta R/(R^2 - R_0^2)]^{l+1/2}$. Finally, the QE-SP coupling constant, $g_{l,\sigma}$, is a complex function of r_E, δ, and R, which scales with cavity size as Δ^3.[30]

In Figure 5, we apply eq 7 NPoM cavity with $R = 120$ nm and $\delta = 8$ nm, and three different QE positions: gap center

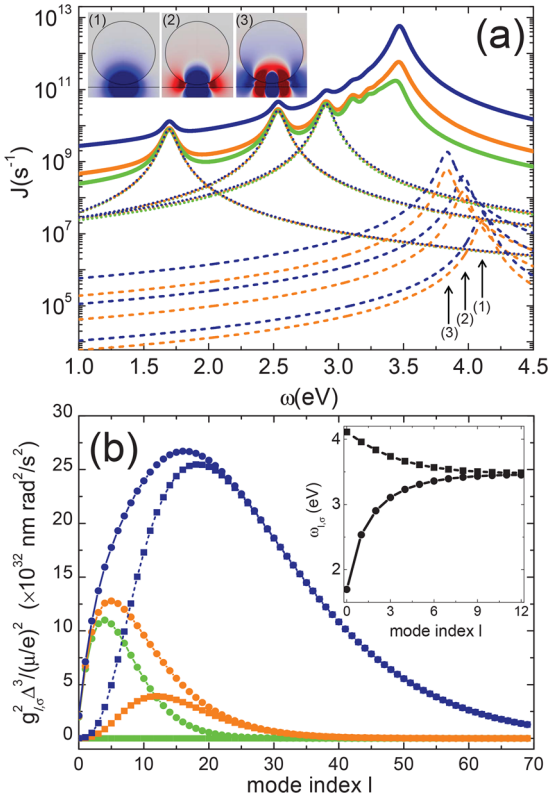

Figure 5. (a) $J(\omega)$ for a NPoM geometry with $R = 120$ nm and $\delta = 8$ nm. Three emitter positions are considered: 4 nm (green), 2.4 nm (orange), and 1.2 nm (dark blue) away from the planar metallic surface. The contribution due to the 3 lowest-l even (dotted line) and odd (dashed line) SP modes are shown. Insets: Induced charge map for the odd SPs. (b) Normalized coupling constant squared for even (circles) and odd (squares) modes vs l for the three emitter positions. Inset: SP resonant frequency vs l.

(green), 2.4 nm (orange), and 1.2 nm (dark blue) away from the flat surface. Note that $J(\omega)$ is identical when evaluated at the same distances but measured from the particle surface. Panel (a) plots the spectral density for the three configurations, which increases as the QE moves away from the gap center in a similar way as $J(\omega_{PS})$ in Figure 4. The Lorentzian contributions

DOI: 10.1021/acsphotonics.7b00616
ACS Photonics 2018, 5, 177−185

due to the three lowest-l even ($\sigma = 1$) and odd ($\sigma = -1$) SP modes are plotted in dotted and dashed lines, respectively. The former red-shift with increasing l and virtually overlap for the three emitter positions. On the contrary, the latter barely shift with increasing SP angular momentum, and show a clear dependence on r_E. The inset displays induced-charge density maps for the three lowest-l odd SPs.

Figure 5b provides deeper insights into the weight of the different terms in eq 7. It plots the coupling constants squared for the three QE positions in panel (a): circles (squares) correspond to even (odd) SPs. We can identify three mechanisms which explain the enhancement of $J(\omega)$ away from the gap center. Due to symmetry constraints, $g_{l,-1}$ vanishes at this position [the corresponding Lorentizans are absent in panel (a)]. By displacing r_E, plasmon-exciton coupling takes place for the set of odd SP modes too. As the QE approaches the gap end, the maxima of both $g_{l,-1}$ and $g_{l,+1}$ increases drastically and become similar. Moreover, the maximum coupling strength for both parities shifts toward higher l (darker and more confined SPs). Therefore, we can infer that the amplification of light−matter interactions due to the asymmetric positioning of the QE occurs through the PS. This conclusion is in agreement with the fact that the Lorentzian contributions for $\sigma = +1$ in Figure 5a do not depend on r_E. The differences in $J(\omega)$ at low frequencies therefore originate from the tail of the PS peak. The coupling strength phenomenology in Figure 5b reveals that the suppressed quenching recently reported in NPoMs[44] takes only place if the QE is placed in a very particular position: the center of the gap. Due to symmetry constraints, the emitter only interacts with even, low-l SPs in this case, which are inherently radiative (green dots). If the QE is displaced away from this position, it also couples to odd modes with higher-l (orange and dark blue dots), which in turn leads to a dramatic enhancement of radiation quenching in the system.

The inset of Figure 5b enables us to identify which SPs can be considered as part of the pseudomode. It plots $\omega_{l,+1}$ (circles) and $\omega_{l,-1}$ (squares). Even SPs red-shift significantly with increasing l, while odd modes only blue-shift slightly. These different trends originate from the denominator in eq 8, which decreases (increases) with l for $\sigma = +1$ ($\sigma = -1$). For large l, $\xi_l \gg 1$, and we can write $\omega_{PS} \sim \frac{\omega_p}{\sqrt{\epsilon_\infty + \epsilon_D}}$ (note that a large ϵ_D allows red-shifting the pseudomode away from the metal plasma frequency). Therefore, those SPs whose frequency lies within a spectral window of width γ centered at ω_{PS} ($l \gtrsim 5$ for both parities) merge together into the broad PS maximum. Finally, note the similarity between the spectral density decomposition phenomenology in Figure 5 and those previously reported for a dimer of identical nanoparticles,[30] which illustrates again the little impact that geometric asymmetry has in the nanocavity performance.

NANOCAVITIES WITH MATERIAL ASYMMETRY

We explore now plasmon-exciton interactions in plasmonic nanocavities comprising two different materials. First, we study dimers of metallic particles with two different permittivities: the Drude silver considered up to here, and a Drude gold with parameters $\epsilon_\infty = 9.7$, $\omega_p = 8.91$ eV, and $\gamma = 0.08$ eV.[45] The SI discusses specific aspects of the TO description of these systems. Figure 6a shows the spectral density along the 2 nm gap of a dimer with $R_1 = R_2 = 120$ nm. The sphere at $z = 0$ ($z = 2R + \delta$), labeled as 2 (1), is made of gold (silver). We can observe that material asymmetry in this nanocavity leads to the

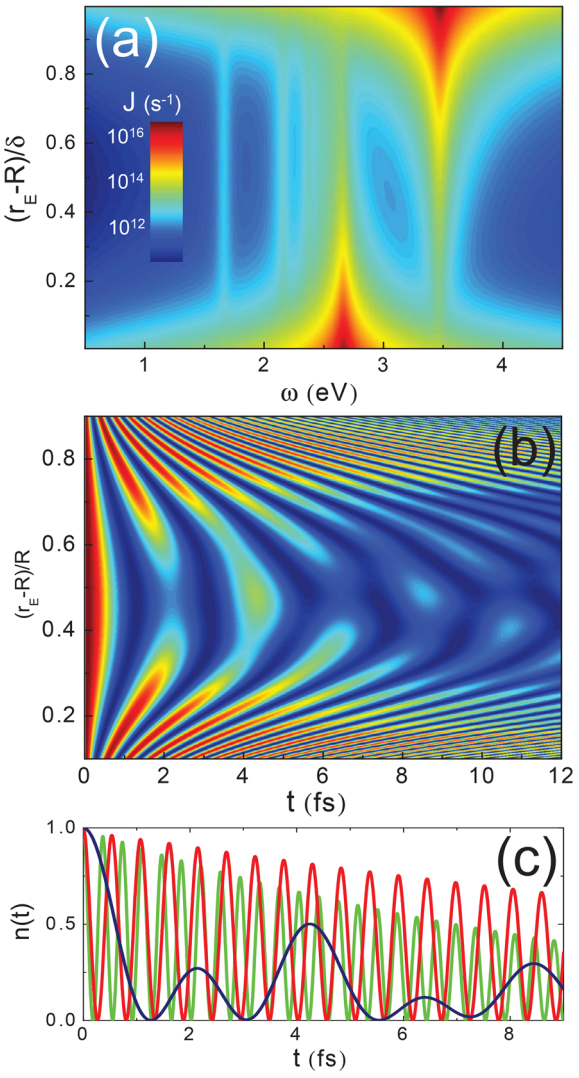

Figure 6. (a) Normalized $J(\omega)$ of Au−Ag nanocavity vs frequency and QE position $(r_E - R)/\delta$ ($R = 120$ nm, $\delta = 2$ nm). (b) Exciton population vs time and QE position for $\omega_E = 3$ eV. The colors render $n(t)$ in linear scale from 0 (dark blue) to 1 (red). (c) $n(t)$ for $(r_E - R)/\delta = 0.1$ (red), 0.5 (dark blue) and 0.9 (green).

emergence of two different pseudomodes in the spectral density map (one associated with each Drude permittivity). Whereas both PSs have a similar contribution at the gap center, $J(\omega)$ is largely determined by one of the PSs as the QE approaches the gap ends. On the contrary, and due to their bright, weakly localized nature, the low-frequency SP peaks below the lowest PS maximum (note that there are no SP peaks between the two pseudomodes) do not exhibit any dependence on the QE position.

The asymmetry in the spatial profile of $J(\omega)$ in Figure 6a can, in principle, be used to tune the dynamics of the exciton population at the QE in space. This possibility is explored in Figure 6b, which displays $n(t)$ obtained from the numerical solution of eq 6 as a function of time and r_E. In order to investigate the interplay between both PSs, we set $\omega_E = 3$ eV, which is in between $\omega_{PS,Au} = 2.6$ eV and $\omega_{PS,Ag} = 3.4$ eV. The contour plot shows that reversible dynamics becomes apparent when the QE approaches the metallic particles. Contrary to $n(t)$ in cavities with geometric asymmetry, the period of these oscillations varies when swapping the QE between symmetric positions

DOI: 10.1021/acsphotonics.7b00616
ACS Photonics 2018, 5, 177−185

with respect to the gap center. At the center, $n(t)$ undergoes a more complex strong-coupling-like evolution. Figure 6c plots cuts of Figure 6b at three different r_Es. Red and green lines are evaluated at a distance 0.1δ away from the Au and Ag sphere surfaces, respectively. They exhibit periodic Rabi oscillations, which are faster close to the silver sphere (due to the larger value of $J(\omega_{PS,Ag})$). Interestingly, when the QE is at the gap center, two different beating frequencies are discernible in $n(t)$. These emerge as a result of the similar plasmon-exciton coupling strengths to the two pseudomodes supported by the cavity.

The SI provides a detailed derivation of the Lorentzian decomposition of $J(\omega)$ for cavities with asymmetric material characteristics. Contrary to homogeneous structures, the splitting of the spectral density contribution for a given l (which leads to the introduction of index σ) can no longer be carried out in an analytical fashion. Instead, the calculation of the SP resonant frequencies, $\omega_{l,\sigma}$ must be performed iteratively. Once these are known, we can write

$$J(\omega) = \sum_{l=0}^{\infty}\sum_{\sigma=1}^{2} \frac{g_{l,\sigma}^2}{\pi} \frac{\gamma_\sigma/2}{(\omega-\omega_{l,\sigma})^2 + (\gamma_\sigma/2)^2} \tag{9}$$

Note that σ does not range from -1 to 1 now. This index still reflects the parity of the SP modes with respect to the gap center. However, in our description of material asymmetry, the two possible values of σ appear closely linked to the two permittivities involved, $\epsilon_1(\omega)$ and $\epsilon_2(\omega)$. Therefore, borrowing the notation introduced in Figure 1a, we have made $\sigma = 1, 2$. Importantly, whereas the width of all Lorentzians were the same in eq 7, two different widths, γ_σ, are present in eq 9. These are given by the Drude damping rates of the two metals involved in the cavity. Once the SP complex frequencies are known, the coupling strengths can be calculated using the high-quality resonator limit.[40]

Figure 7a plots $J(\omega)$ at the gap center for the nanocavity in Figure 6. The spectral density decomposition given by eq 9 is plotted in black solid line, showing an excellent agreement with the exact TO calculation, in gray dashed line. The Lorentzian contributions for $0 \le l \le 2$ and for $\sigma = 1$ (odd modes, linked to Ag permittivity) and $\sigma = 2$ (even modes, linked to Au permittivity) are shown in orange and blue dashed lines, respectively. In order to unveil the fingerprint of the PSs corresponding to both metals in $J(\omega)$, orange and blue solid lines render the spectral densities for single Ag and Au particles. We can observe that while even modes are significantly red-shifted with respect to $\omega_{PS,Au}$, odd modes are located in the vicinity of $\omega_{PS,Ag}$. Figure 7b,c render SP resonant frequencies and coupling strengths, respectively, as a function of index l. Solid dots plot fully converged $\omega_{l,\sigma}$ and $g_{l,\sigma}^2$ (~10 iterations), whereas empty dots correspond to their zero-order approximation, see SI for more details. For large l, both quantities are correctly described without the need of any iteration in our calculations (note that the seed for the SP-frequencies is set at the PS of the spheres isolated). Only for low l, SP fields extend far from the nanoparticles. This gives rise to strong plasmonic hybridization effects across the gap, whose description requires a number of iterations in our approach. Remarkably, Figure 7c demonstrates that, contrary to geometric asymmetry, the introduction of material asymmetry in the nanocavity leads to a nonvanishing coupling strength between low-l, odd ($\sigma = 1$) SPs and QEs placed at the gap center.

Our TO approach can also be applied to metal-dielectric cavities, in which the dielectric constant of the nonmetallic sphere,

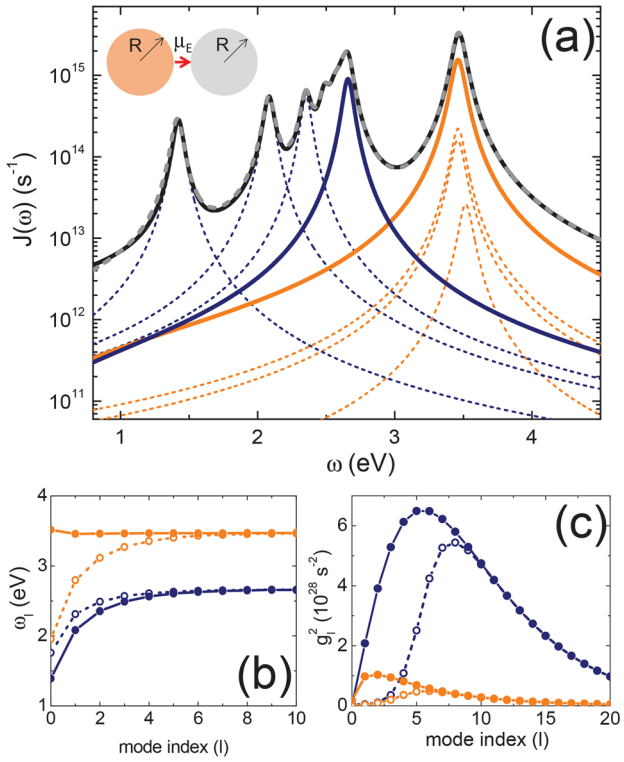

Figure 7. (a) Exact spectral density (gray dashed line) and its analytical decomposition (black solid line) at the gap center of a Au−Ag nanocavity (R = 120 nm, δ = 2 nm). Dotted lines plot the contribution for the 3 lowest even (dark blue) and odd (orange) SP modes. $J(\omega)$ for a single Au (Ag) sphere is shown in dark blue (orange) solid line. (b) SP frequencies as a function of the mode index. (c) Coupling constant squared as a function of the mode index. Empty and solid dots in these two panels show zero-order iteration calculations and fully converged results, respectively.

ϵ_2, is large enough to avoid significant radiative losses. In this configuration, as discussed in the SI, the cavity supports only one set of SP modes. This makes the index σ in eq 9 redundant. Importantly, as in the case of single metal dimers, the SP frequencies in a metal-dielectric nanocavity, ω_l, can be calculated analytically without any iterative procedure. Thus, we obtain an expression for the SP resonant frequencies of the form of eq 8 evaluated at $\sigma = 1$ and $\xi_l = \xi_l(\epsilon_2) = \left(\frac{\epsilon_2+\epsilon_D}{\epsilon_2-\epsilon_D}\right)\left(\frac{1+\Delta_2}{1-\Delta_1}\right)^{l+1/2}$.

In Figure 8, we investigate the spectral density at the center of the 2 nm gap between silver and dielectric spheres of 120 nm radius. Four different values of ϵ_2 are shown: 4 (orange), 6 (green), 9 (red), and 15 (dark blue). For comparison, the spectral density for a single silver sphere is plotted in gray solid line ($\epsilon_2 = \epsilon_D = 2.13$). On the one hand, it is evident that the presence of the dielectric sphere does not modify $J(\omega_{PS})$, which is extremely similar in the five configurations considered. On the other hand, we can observe that by increasing the dielectric permittivity, low frequency maxima emerge in $J(\omega)$. These peaks grow and red-shift with larger ϵ_2. Thus, we can infer that the neighboring dielectric particle only enhances the QE coupling to low frequency SPs. This conclusion is supported by the left top inset of Figure 8, which plots g_l^2 (obtained from the decomposition of the spectra in the main panel) versus l. It shows that only the coupling strengths for $l < 10$ increase (up to a factor ~ 2) with larger dielectric constant. Finally, the right bottom inset displays a color-saturated induced charge density map for

DOI: 10.1021/acsphotonics.7b00616
ACS Photonics 2018, 5, 177−185

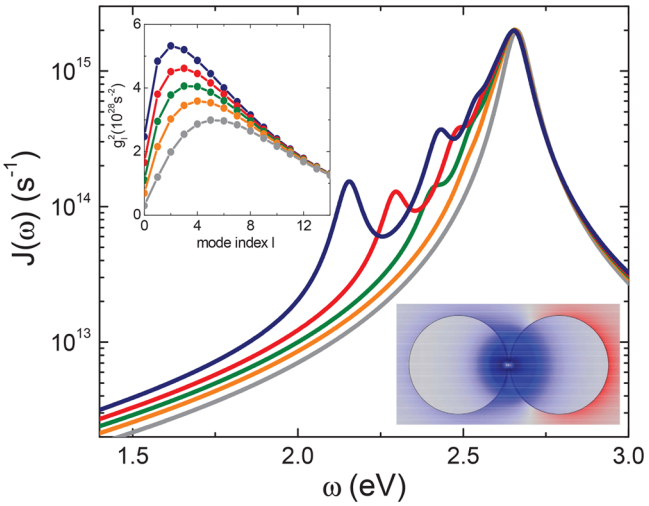

Figure 8. Spectral density for silver-dielectric nanocavities with R = 120 nm and δ = 2 nm. Four dielectric constants, ϵ_2, are considered: 4 (orange), 6 (green), 9 (red), and 15 (dark blue). $J(\omega)$ for a single Ag sphere is shown in gray. Top left inset: Coupling constant squared as a function of the mode index for the five cases in the main panel. Bottom right inset: Induced charge density map for the lowest SP mode (ω = 2.2 eV) and ϵ_2 = 15.

ϵ_2 = 15 evaluated at ω = 2.2 eV. We can identify the SP mode responsible for the lowest frequency maximum in $J(\omega)$ with the dipole SP sustained by the isolated Ag nanoparticle. The presence of the dielectric sphere only modifies the spatial profile of the SPs quantitatively, but they remain qualitatively the same.

CONCLUSION

In conclusion, we have presented a transformation optics description of plasmon-exciton strong coupling in symmetry-broken nanocavities at the single emitter level. We have investigated plasmonic systems presenting geometric asymmetry, such as nanoparticle-on-a-mirror configurations, and material asymmetry, such as metal−metal and metal-dielectric dimers. Our method provides a quasi-analytical description of the spectral density across the gap of these cavities, and allows for its convenient decomposition as a sum of Lorentzian-like terms. This fact allows us to shed insights into the role that asymmetry plays in the interaction between emitter and cavity, largely governed by the high-frequency pseudomode supported by the latter. On the one hand, our findings reveal that plasmon-exciton interactions exhibit a remarkably low sensitivity to geometric asymmetry. On the other hand, they show that the introduction of material asymmetry can lead to relevant variations in the spatial and spectral strong-coupling phenomenology, which opens new ways for tailoring the properties of plasmon-exciton-polaritons.

ASSOCIATED CONTENT

Supporting Information

The Supporting Information is available free of charge on the ACS Publications website at DOI: 10.1021/acsphotonics.7b00616.

Specific details on the transformation optics description of gap cavities with asymmetric material characteristics (composed of nanospheres of metal−metal or metal−dielectric materials). The first section deals with general aspects of the spectral density calculations. The second section describes the iterative approach followed to obtain quasi-analytical expressions for the surface plasmon resonant frequencies in these systems (PDF).

AUTHOR INFORMATION

Corresponding Author

*E-mail: a.fernandez-dominguez@uam.es.

ORCID

A. I. Fernández-Domínguez: 0000-0002-8082-395X

Notes

The authors declare no competing financial interest.

ACKNOWLEDGMENTS

This work has been funded by the EU Seventh Framework Programme under Grant Agreement FP7-PEOPLE-2013-CIG-630996, the European Research Council (ERC-2011-AdG Proposal No. 290981), and the Spanish MINECO under Contracts FIS2015-64951-R, MAT2014-53432-C5-5-R, and through the "María de Maeztu" programme for Units of Excellence in R&D (MDM-2014-0377). R.-Q.L. acknowledges funding by the China Scholarship Council and thanks Prof. Jian-Chun Cheng for guidance and support. All the authors thank Álvaro Cuartero-González for fruitful discussions.

REFERENCES

(1) Tame, M. S.; McEnery, K. R.; Özdemir, S. K.; Lee, J.; Maier, S. A.; Kim, M. S. Quantum Plasmonics. *Nat. Phys.* **2013**, *9*, 329−340.

(2) Fernández-Domínguez, A. I.; García-Vidal, F. J.; Martín-Moreno, L. Unrelenting Plasmons. *Nat. Photonics* **2017**, *11*, 8−10.

(3) Maier, S. A. *Plasmonics: Fundamentals and Applications*; Springer: New York, 2007.

(4) Chang, D. E.; Sorensen, A. S.; Hemmer, P. R.; Lukin, M. D. Quantum Optics with Surface Plasmons. *Phys. Rev. Lett.* **2006**, *97*, 053002.

(5) Törmä, P.; Barnes, W. L. Strong Coupling between Surface Plasmon Polaritons and Emitters: a Review. *Rep. Prog. Phys.* **2015**, *78*, 013901.

(6) Salomon, A. R.; Gordon, J.; Prior, Y.; Seideman, T.; Sukharev, M. Strong Coupling between Molecular Excited States and Surface Plasmon Modes of a Slit Array in a Thin Metal Film. *Phys. Rev. Lett.* **2012**, *109*, 073002.

(7) González-Tudela, A.; Huidobro, P. A.; Martín-Moreno, L.; Tejedor, C.; García-Vidal, F. J. Theory of Strong Coupling between Quantum Emitters and Propagating Surface Plasmons. *Phys. Rev. Lett.* **2013**, *110*, 126801.

(8) Delga, A.; Feist, J.; Bravo-Abad, J.; García-Vidal, F. J. Quantum Emitters Near a Metal Nanoparticle: Strong Coupling and Quenching. *Phys. Rev. Lett.* **2014**, *112*, 253601.

(9) Bellessa, J.; Bonn, C.; Plenet, J. C.; Mugnier, J. Strong Coupling between Surface Plasmons and Excitons in an Organic Semiconductor. *Phys. Rev. Lett.* **2004**, *93*, 036404.

(10) Schwartz, T.; Hutchison, J. A.; Genet, C.; Ebbesen, T. W. Reversible Switching of Ultrastrong Light-Molecule Coupling. *Phys. Rev. Lett.* **2011**, *106*, 196405.

(11) Zengin, G.; Wersäll, M.; Nilsson, S.; Antosiewicz, T. J.; Käll, M.; Shegai, T. Realizing Strong Light−Matter Interactions between Single-Nanoparticle Plasmons and Molecular Excitons at Ambient Conditions. *Phys. Rev. Lett.* **2015**, *114*, 157401.

(12) Todisco, F.; D'Agostino, S.; Esposito, M.; Fernández-Domínguez, A. I.; De Giorgi, M.; Ballarini, D.; Dominici, L.; Tarantini, I.; Cuscuna, M.; Della Sala, F.; Gigli, G.; Sanvitto, D. Exciton-Plasmon Coupling Enhancement via Metal Oxidation. *ACS Nano* **2015**, *9*, 9691−9699.

(13) Todisco, F.; Esposito, M.; Panaro, S.; De Giorgi, M.; Dominici, L.; Ballarini, D.; Fernández-Domínguez, A. I.; Tasco, V.; Cuscuna, M.; Passaseo, A.; Ciraci, C.; Gigli, G.; Sanvitto, D. Toward Cavity

DOI: 10.1021/acsphotonics.7b00616
ACS Photonics 2018, 5, 177−185

Quantum Electrodynamics with Hybrid Photon Gap-Plasmon States. *ACS Nano* **2016**, *10*, 11360−11368.
(14) Ramezani, M.; Halpin, A.; Fernández-Domínguez, A. I.; Feist, J.; Rodríguez, S. R.-K.; García-Vidal, F. J.; Gómez-Rivas, J. Plasmon-Exciton-Polariton Lasing. *Optica* **2017**, *4*, 31−37.
(15) Hutchison, J. A.; Schwartz, T.; Genet, C.; Devaux, E.; Ebbesen, T. W. Modifying Chemical Landscapes by Coupling to Vacuum Fields. *Angew. Chem., Int. Ed.* **2012**, *51*, 1592−1596.
(16) Galego, J.; García-Vidal, F. J.; Feist, J. Suppressing Photochemical Reactions with Quantized Light Fields. *Nat. Commun.* **2016**, *7*, 13841.
(17) Feist, J.; García-Vidal, F. J. Extraordinary Exciton Conductance Induced by Strong Coupling. *Phys. Rev. Lett.* **2015**, *114*, 196402.
(18) Orgiu, E.; George, J.; Hutchison, J. A.; Devaux, E.; Dayen, J. F.; Doudin, B.; Stellacci, F.; Genet, C.; Schachenmayer, J.; Genes, C.; Pupillo, G.; Samorí, P.; Ebbesen, T. W. Conductivity in Organic Semiconductors Hybridized with the Vacuum Field. *Nat. Mater.* **2015**, *14*, 1123−1129.
(19) Hartsfield, T.; Chang, W.-S.; Yang, S.-C.; Ma, T.; Shi, J.; Sun, L.; Shvets, G.; Link, S.; Li, X. Single Quantum Dot Controls a Plasmonic Cavity's Scattering Anisotropy. *Proc. Natl. Acad. Sci. U. S. A.* **2015**, *112*, 12288−12292.
(20) Gong, S.-H.; Kim, J.-H.; Ko, Y.-H.; Rodríguez, C.; Shin, J.; Lee, Y.-H.; Dang, L. S.; Zhang, X.; Cho, Y.-H. Self-aligned Deterministic Coupling of Single Quantum Emitter to Nanofocused Plasmonic Modes. *Proc. Natl. Acad. Sci. U. S. A.* **2015**, *112*, 5280−5285.
(21) Hoang, T. B.; Akselrod, G. M.; Mikkelsen, M. H. Ultrafast Room-Temperature Single Photon Emission from Quantum Dots Coupled to Plasmonic Nanocavities. *Nano Lett.* **2016**, *16*, 270−275.
(22) Chikkaraddy, R.; de Nijs, B.; Benz, F.; Barrow, S. J.; Scherman, O. A.; Rosta, E.; Demetriadou, A.; Fox, P.; Hess, O.; Baumberg, J. J. Single-Molecule Strong Coupling at Room Temperature in Plasmonic Nanocavities. *Nature* **2016**, *535*, 127−130.
(23) Santhosh, K.; Bitton, O.; Chuntonov, L.; Haran, G. Vacuum Rabi Splitting in a Plasmonic Cavity at the Single Quantum Emitter Limit. *Nat. Commun.* **2016**, *7*, 11823.
(24) González-Tudela, A.; Huidobro, P. A.; Martín-Moreno, L.; Tejedor, C.; García-Vidal, F. J. Reversible Dynamics of Single Quantum Emitters near Metal-Dielectric Interfaces. *Phys. Rev. B: Condens. Matter Mater. Phys.* **2014**, *89*, 041402.
(25) Ridolfo, A.; Di Stefano, O.; Fina, N.; Saija, R.; Savasta, S. Quantum Plasmonics with Quantum Dot-Metal Nanoparticle Molecules: Influence of the Fano Effect on Photon Statistics. *Phys. Rev. Lett.* **2010**, *105*, 263601.
(26) Varguet, H.; Rousseaux, B.; Dzsotjan, D.; Jauslin, H. R.; Guérin, S.; Colas des Francs, G. Dressed states of a quantum emitter strongly coupled to a metal nanoparticle. *Opt. Lett.* **2016**, *41*, 4480−4483.
(27) Savasta, S.; Saija, R.; Ridolfo, A.; Di Stefano, O.; Denti, P.; Borghese, F. Nanopolaritons: Vacuum Rabi Splitting with a Single Quantum Dot in the Center of a Dimer Nanoantenna. *ACS Nano* **2010**, *4*, 6369−6376.
(28) Manjavacas, A.; García de Abajo, F. J.; Nordlander, P. Quantum Plexcitonics: Strongly Interacting Plasmons and Excitons. *Nano Lett.* **2011**, *11*, 2318−2323.
(29) Pendry, J. B.; Schurig, D.; Smith, D. R. Controlling Electromagnetic Fields. *Science* **2006**, *312*, 1780−1782.
(30) Li, R.-Q.; Hernangómez-Pérez, D.; García-Vidal, F. J.; Fernández-Domínguez, A. I. Transformation Optics Approach to Plasmon-Exciton Strong Coupling in Nanocavities. *Phys. Rev. Lett.* **2016**, *117*, 107401.
(31) Luo, Y.; Zhao, R.; Fernández-Domínguez, A. I.; Pendry, J. B. Harvesting Light with Transformation Optics. *Sci. China Inf. Sci.* **2013**, *56*, 120401.
(32) Zhao, R.; Luo, Y.; Fernández-Domínguez, A. I.; Pendry, J. B. Description of van der Waals Interactions Using Transformation Optics. *Phys. Rev. Lett.* **2013**, *111*, 033602.
(33) Fernández-Domínguez, A. I.; Wiener, A.; García-Vidal, F. J.; Maier, S. A.; Pendry, J. B. Transformation-Optics Description of Nonlocal Effects in Plasmonic Nanostructures. *Phys. Rev. Lett.* **2012**, *108*, 106802.
(34) Pendry, J. B.; Fernández-Domínguez, A. I.; Luo, Y.; Zhao, R. Capturing Photons with Transformation Optics. Nat. *Nat. Phys.* **2013**, *9*, 518−522.
(35) Fernández-Domínguez, A. I.; Maier, S. A.; Pendry, J. B. Collection and Concentration of Light by Touching Spheres: A Transformation Optics Approach. *Phys. Rev. Lett.* **2010**, *105*, 266807.
(36) Noginov, M. A.; Zhu, G.; Belgrave, A. M.; Bakker, R.; Shalaev, V. M.; Narimanov, E. E.; Stout, S.; Herz, E.; Suteewong, T.; Wiesner, U. Demonstration of a spaser-based nanolaser. *Nature* **2009**, *460*, 1110−1113.
(37) Guest, J. R.; Stievater, T. H.; Li, X.; Cheng, J.; Steel, D. G.; Gammon, D.; Katzer, D. S.; Park, D.; Ell, C.; Thränhardt, A.; Khitrova, G.; Gibbs, H. M. Measurement of optical absorption by a single quantum dot exciton. *Phys. Rev. B: Condens. Matter Mater. Phys.* **2002**, *65*, 241310.
(38) Novotny, L.; Hecht, B. *Principles of Nano-Optics*; Cambridge University Press: Cambridge, 2012.
(39) Breuer, H.-P.; Petruccione, F. *The Theory of Open Quantum Systems*; Oxford University Press: Oxford, 2002.
(40) Waks, E.; Sridharan, D. Cavity QED Treatment of Interactions between a Metal Nanoparticle and a Dipole Emitter. *Phys. Rev. A: At., Mol., Opt. Phys.* **2010**, *82*, 043845.
(41) Sauvan, C.; Hugonin, J. P.; Maksymov, I. S.; Lalanne, P. Theory of the Spontaneous Optical Emission of Nanosize Photonic and Plasmon Resonators. *Phys. Rev. Lett.* **2013**, *110*, 237401.
(42) Doost, M. B.; Langbein, W.; Muljarov, E. A. Resonant-State Expansion Applied to Three-Dimensional Open Optical Systems. *Phys. Rev. A: At., Mol., Opt. Phys.* **2014**, *90*, 013834.
(43) Kristensen, P. T.; Hughes, S. Modes and Mode Volumes of Leaky Optical Cavities and Plasmonic Nanoresonators. *ACS Photonics* **2014**, *1*, 2−10.
(44) Kongsuwan, N.; Demetriadou, A.; Chikkaraddy, R.; Benz, F.; Turek, V. A.; Keyser, U. F.; Baumberg, J. J.; Hess, O. Suppressed Quenching and Strong Coupling of Purcell-Enhanced Single-Molecule Emission in Plasmonic Nanocavities. *arXiv:physics/1612.02611* 2017; https://arxiv.org/abs/1612.02611 (accessed June, 13, 2017).
(45) Vial, A.; Grimault, A.-S.; Macías, D.; Barchiesi, D.; Lamy de la Chapelle, M. Improved Analytical Fit of Gold Dispersion: Application to the Modeling of Extinction Spectra with a Finite-Difference Time-Domain Method. *Phys. Rev. B: Condens. Matter Mater. Phys.* **2005**, *71*, 085416.

DOI: 10.1021/acsphotonics.7b00616
ACS Photonics 2018, 5, 177−185